Supporting Information for

Chiral molecular face-rotating sandwich structures constructed through restricting phenyl flipping of tetraphenylethylene

Hang Qu,[a+] Xiao Tang,[a+] Xinchang Wang,[a] Zhihao Li,[a] Zheyu Huang,[a] Hui Zhang,[a] Zhongqun Tian,[a] and Xiao-Yu Cao [a*]

[a] State Key Laboratory of Physical Chemistry of Solid Surfaces, Key Laboratory of Chemical Biology of Fujian Province, Collaborative Innovation Center of Chemistry for Energy Materials (iChEM) and College of Chemistry and Chemical Engineering, Xiamen University, Xiamen 361005 (P. R. China).

* Email: xcao@xmu.edu.cn

[+] These authors contribute equally to this work.

1. Instruments and Materials

General. All commercially available chemicals were used without further purification unless otherwise noted. And solvents used in synthesis processes were purified by reflux in the presence of Na or $CaCl_2$ prior to use.

HPLC analyses were performed on a Shimadazu LC-16A instrument with Daicel Chiralpak IE Column. High-resolution mass spectra (HRMS) were recorded on a Bruker En Apex Ultra 7.0T FT-MS mass spectrometer. Absorption spectra were recorded on Shimadzu UV2700 UV-vis spectrometer. CD spectra were recorded on JASCO J-810 circular dichroism spectrometer at 298K. ^{1}H- and ^{13}C-NMR spectra were recorded on a Bruker AVIII-500 spectrometer (500 and 125 MHz, respectively) or a Bruker AVIII-850 spectrometer (850 and 213 MHz, respectively) at 298 K. Chemical shifts were reported in ppm. Coupling constants (J values) were reported in Hertz.

A list of abbreviations：

rt: room temperature

DCM: dichloromethane

DMF: N,N-dimethylformamide

DMSO: dimethyl sulfoxide

EA: ester acetate

PE: petrol ether

THF: tetrahydrofuran

CD: circular dichroism

HPLC: high-performance liquid chromatography

NMR: nuclear magnetic resonance

DEPT: distortionless enhancement by polarization transfer

COSY: correlation spectroscopy

HSQC: heteronuclear single-quantum correlation

HMBC: ^{1}H detected heteronuclear multiple bond correlation

NOESY: nuclear Overhauser enhancement spectroscopy

ESI-HRMS: electrospray ionization high resolution mass spectrometry

MALDI-TOF: matrix-assisted laser desorption/ionization-time of flight mass spectrometry

2. Supplementary Figures

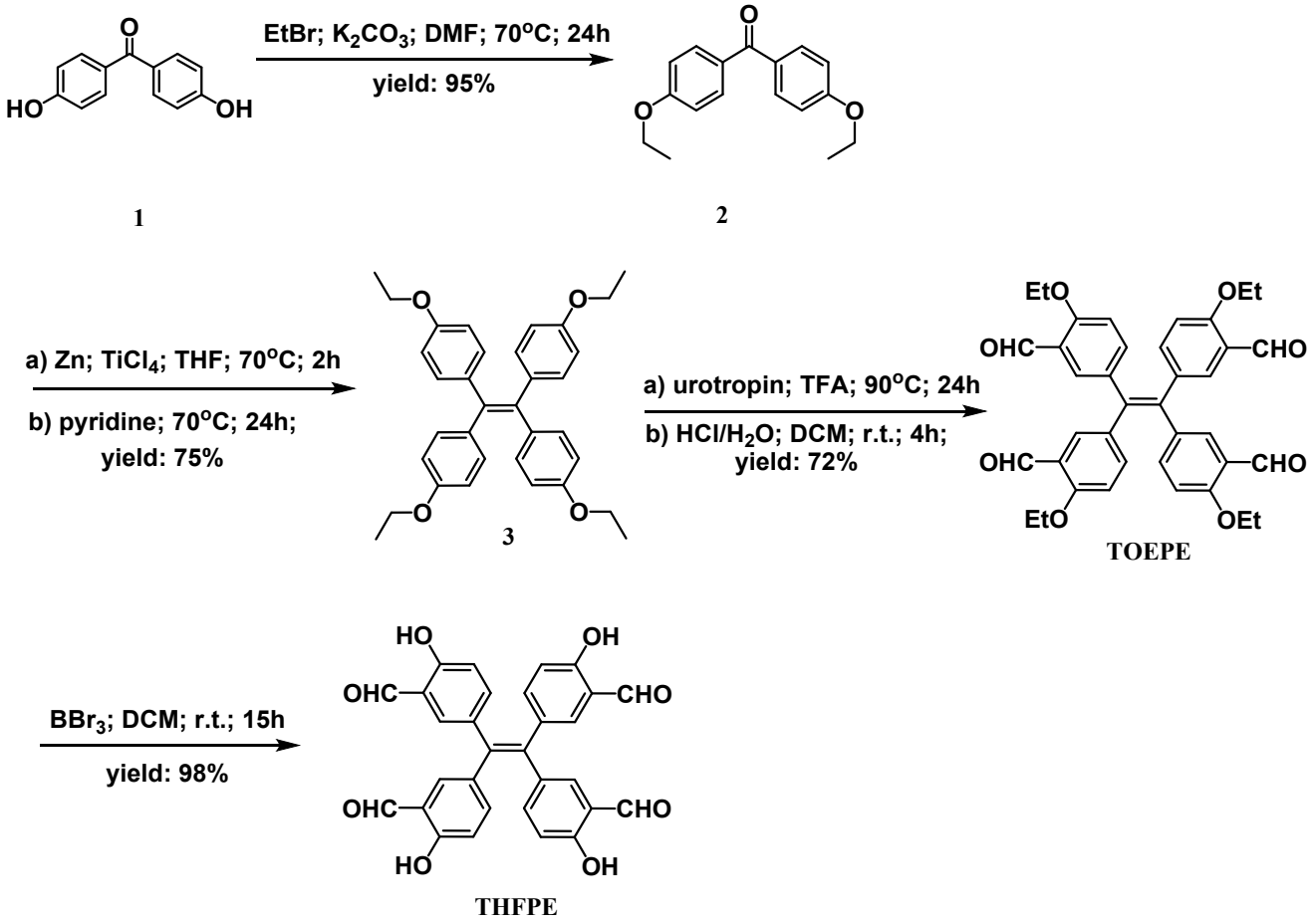

Figure S1. Synthesis of 1,1,2,2-tetrakis(4-hydroxyl-3-formylphenyl)ethene (THFPE).

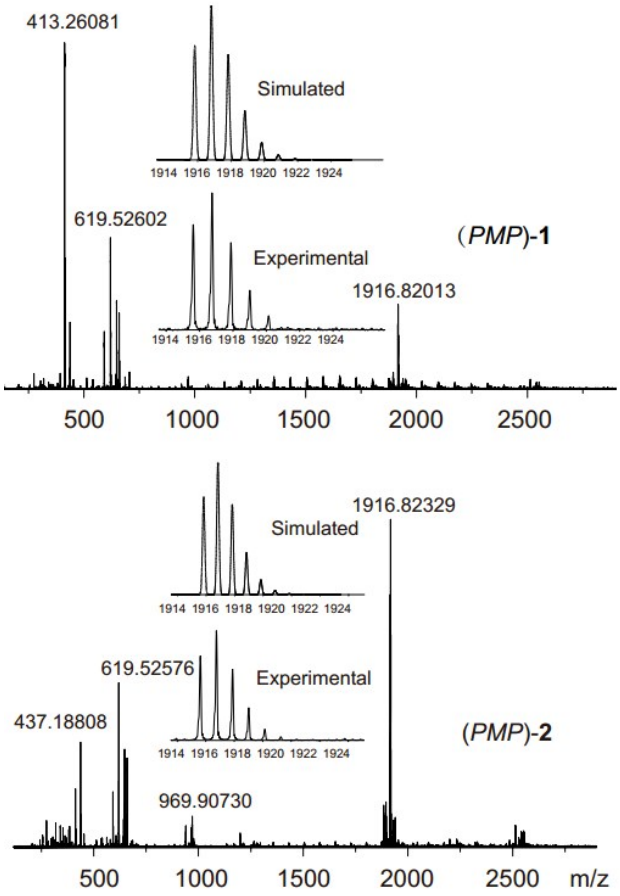

Figure S2. ESI-HRMS spectra of *PMP*-**1** (top) and *PMP*-**2** (bottom). And the insert images show the simulated and experimental isotopic distributions of $[C_{114}H_{108}O_{12}N_{16} + Na]^+$ species of *PMP*-**1** and *PMP*-**2**, respectively.

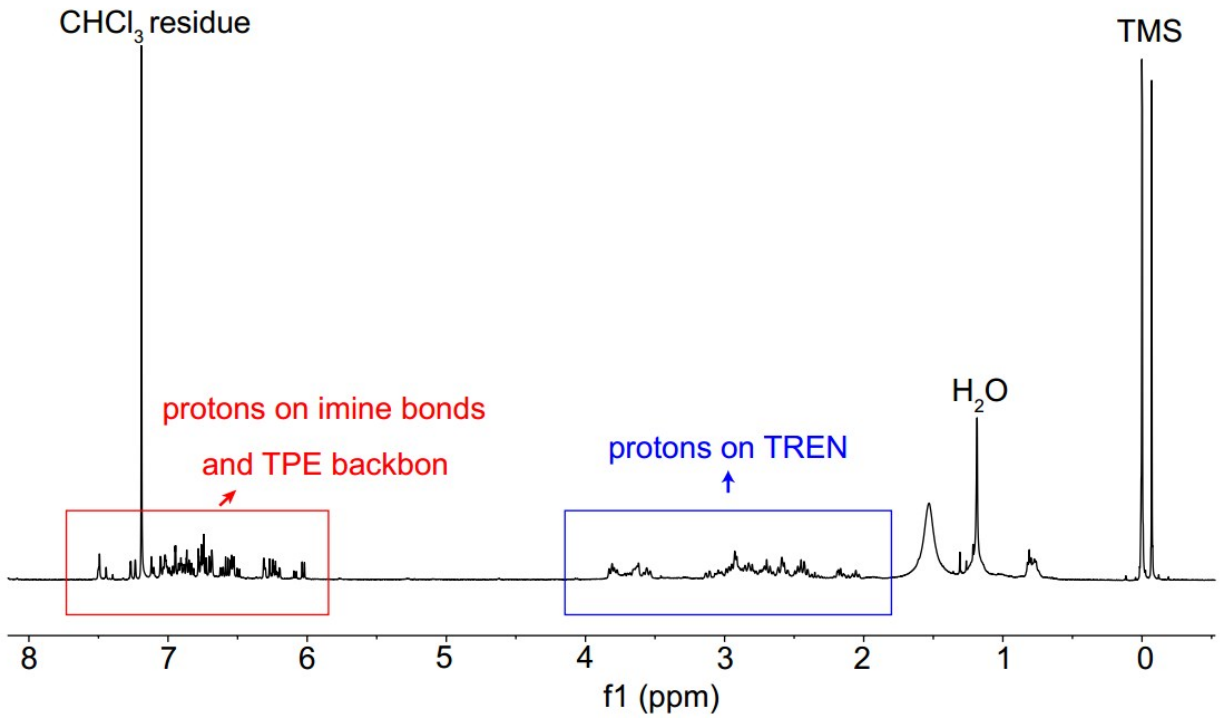

Figure S3. Initial ^{1}H-NMR spectrum of crude solution (500 MHz).

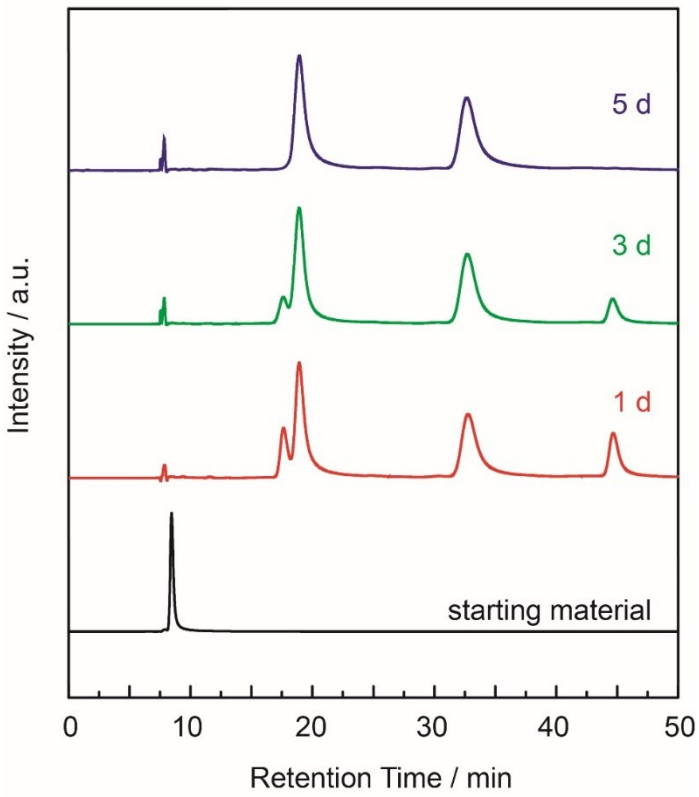

Figure S4. Kinetic experiments of the reaction monitored by HPLC spectra.

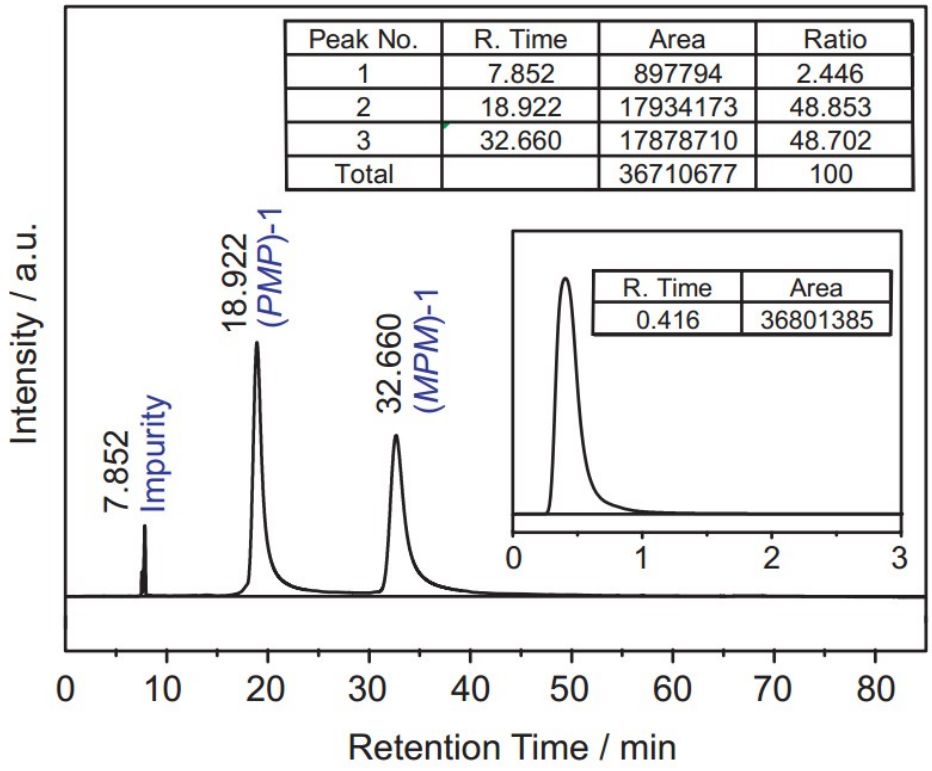

Figure S5. The full chiral HPLC spectrum showed that the final products only contained two chiral enantiomers, *PMP*-**1** and *MPM*-**1** in a 1:1 ratio. As a comparison, we performed an analysis without chiral column (the inset spectrum), wherein peak area (3.68×10^7) matched well with the overall peak area of fractions in column analysis (3.67×10^7). According to above data, the yield of each enantiomers can be calculated as 48.853% and 48.702% corresponding to *PMP*-**1** and *MPM*-**1**, respectively. And the total reaction yield was 97.6%.

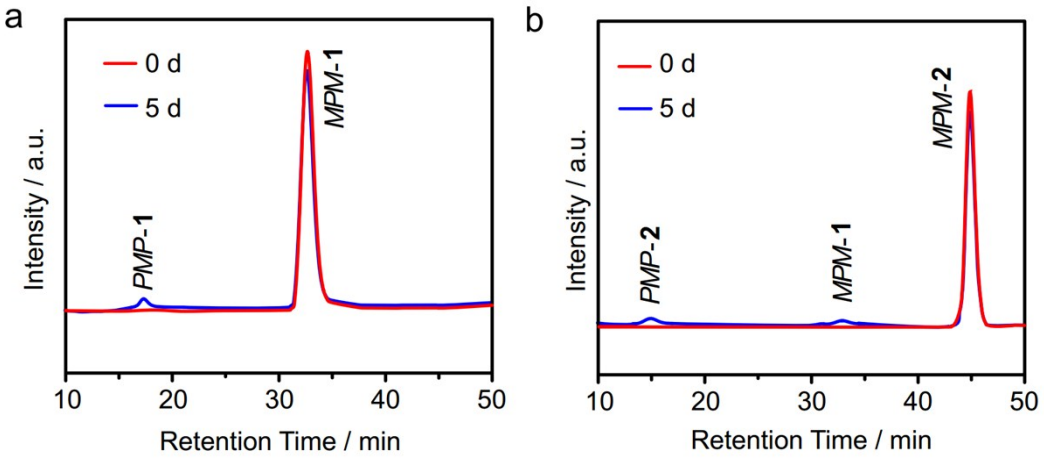

Figure S6. Time-dependent chiral-HPLC analyses for determining the racemization time. HPLC spectra of *MPM*-**1** (a, red) and after 5 days (a, blue)**.** HPLC spectra of *MPM*-**2** (b, red) and after 5 days (b, blue).

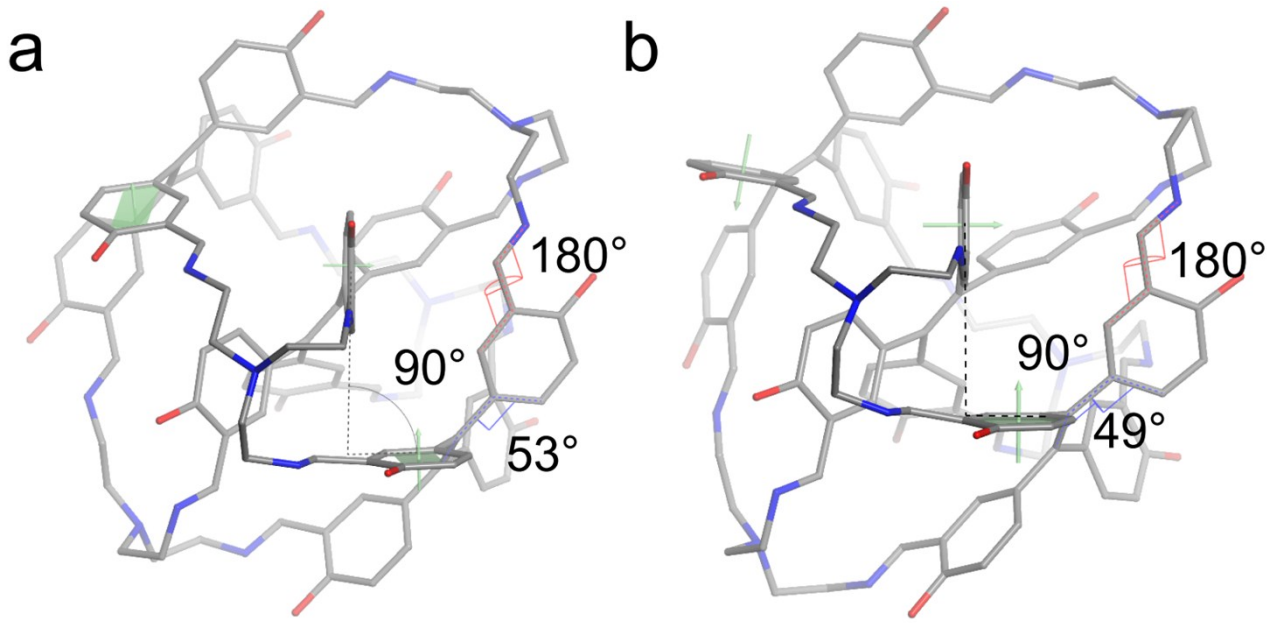

Figure S7. Crystal structures of *PMP*-**1** (a) and *PMP*-**2** (b) to illustrate the dihedral angles (C_{Ar}-C_{Ar}-C-C) between vinyl bonds and phenyl rings (blue line), the dihedral angles of phenyl rings on one vertex (black line) and the dihedral angles between imine bond and adjacent phenyl ring (red line).

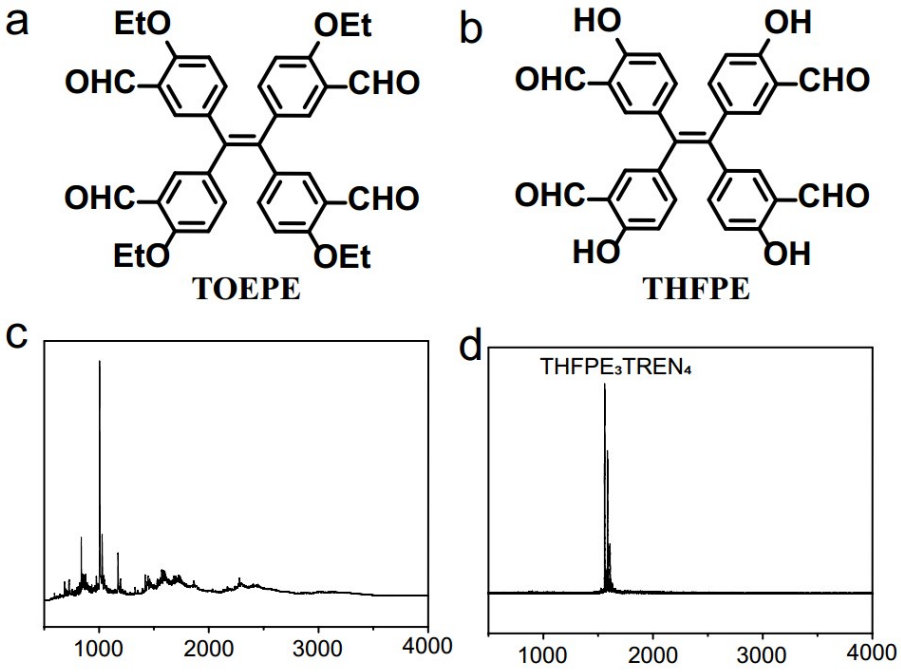

Figure S8. Structural formula of the TOEPE (a) and THFPE (b). MALDI-TOF spectra of crude solution after imine condensation by using TOEPE (c) or THFPE (d).

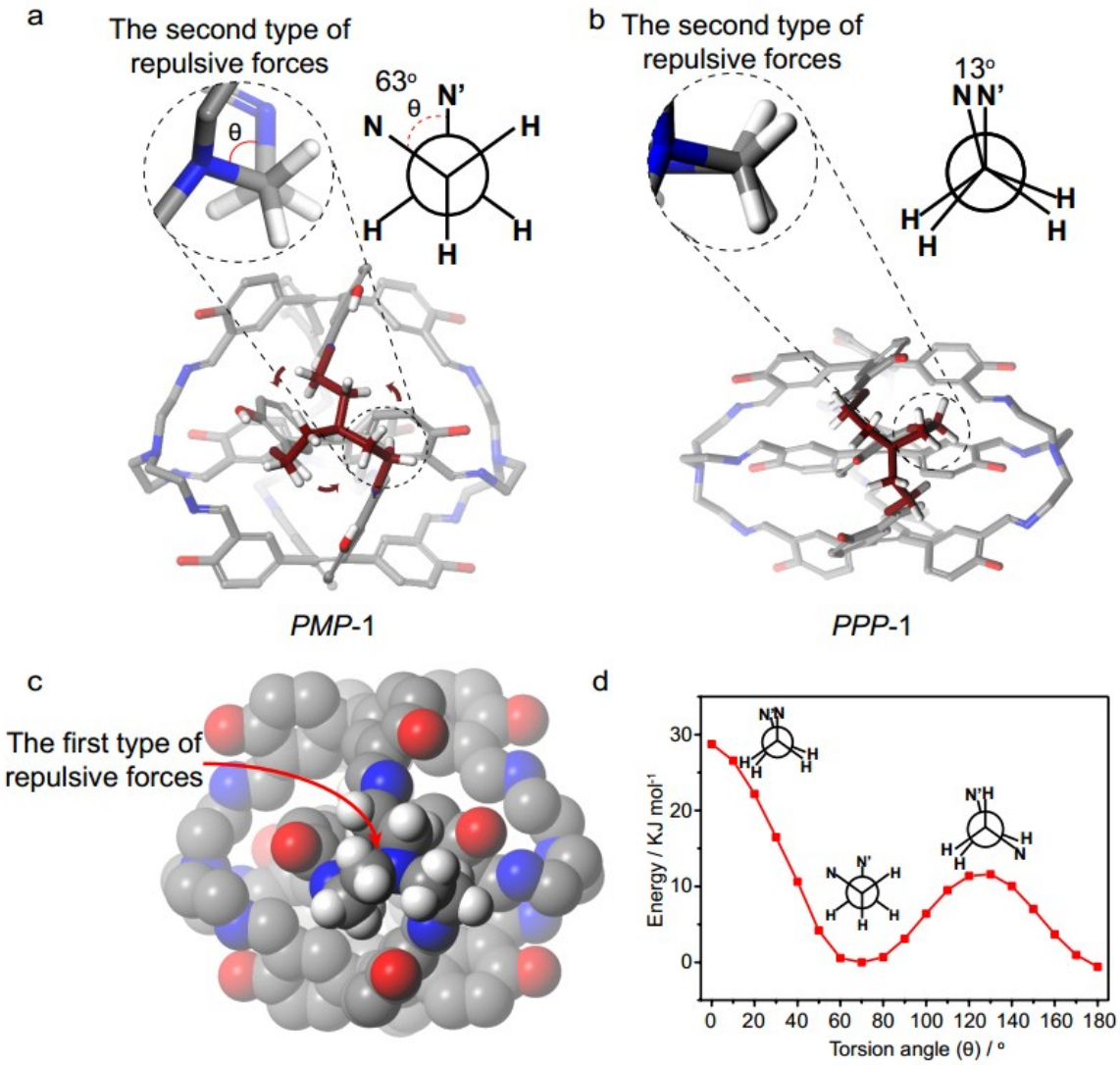

Figure S9. The configurations of TREN resulted in special stacking of TPE units. Single-crystal structure of *PMP*-**1** exhibited anti-clockwise rotational configurations of TREN (a, bottom) (Hydrogen atoms are omitted for clarity expect for one TREN vertex). The N-C-C-N gauche conformation of one alkyl chain in TREN has a 63° torsion angle (θ, a, up), exhibiting the second type of repulsive interactions. In addition, the first type of non-covalent repulsive interactions among three alkyl chains was shown in CPK mode (c). The optimized structure of *PPP*-**1** was built to compare the configurations of TREN to that of *PMP*-**1** (b, bottom). In contrast to the anti-clockwise rotational configuration of TREN in *PMP*-**1**, TREN in the optimized structure of *PPP*-**1** has an extremely distorted configuration, which exhibited strong repulsive interactions. The DFT calculation (d) revealed alkyl chains of *PMP*-**1** have the lowest energy in a 65° torsion angle and transmit the rotational chirality of TREN to TPE units due to the complete coplanarity between imine bonds and phenyl rings. Whereas the alkyl chains of TREN in *PPP*-**1** have a 13° torsion angles, which displayed the highest energy in PES.

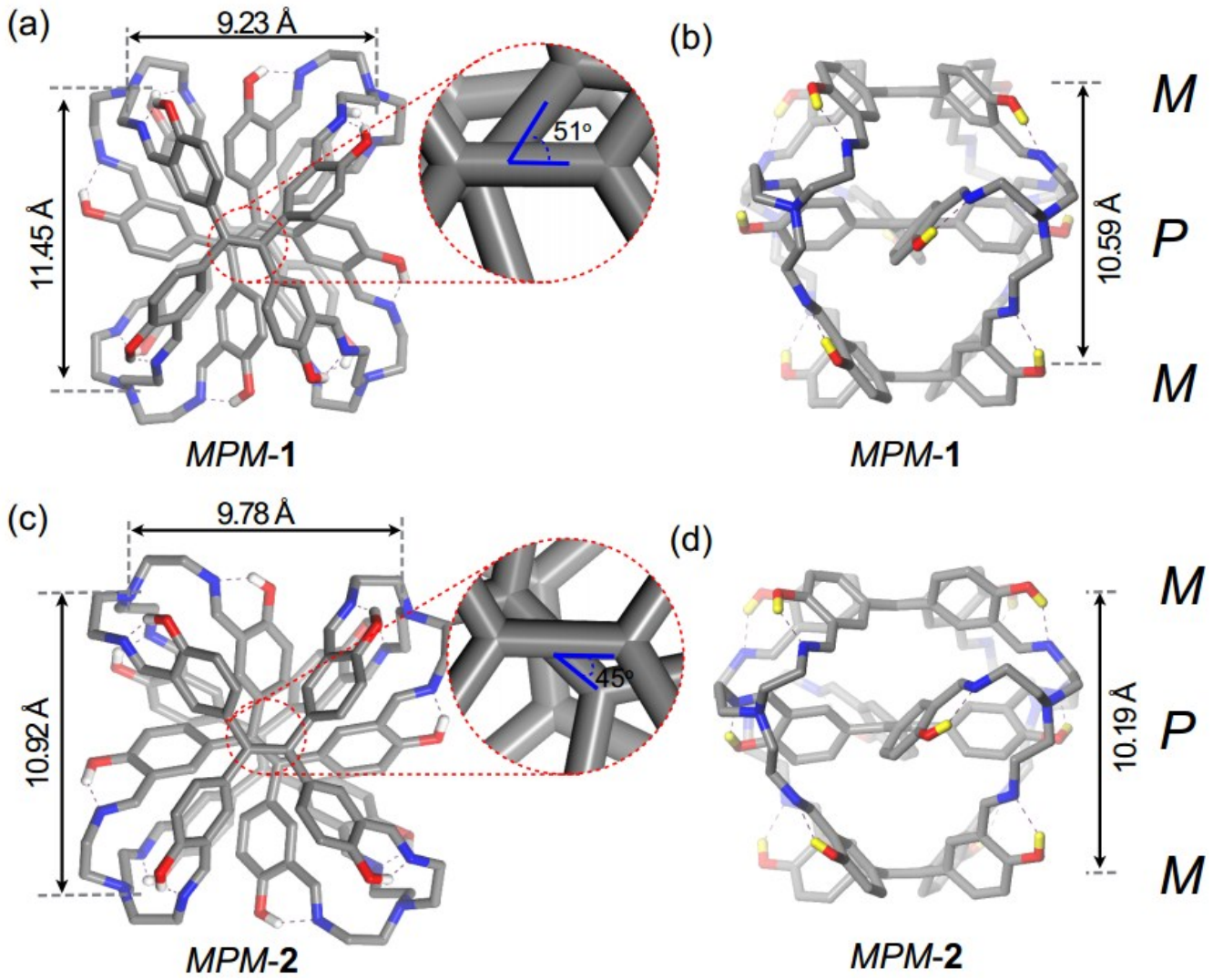

Figure S10. Crystal structures of *MPM*-**1** (a, b) and *MPM*-**2** (c, d), which are the enantiomers of *PMP*-**1** or *PMP*-**2**, respectively.

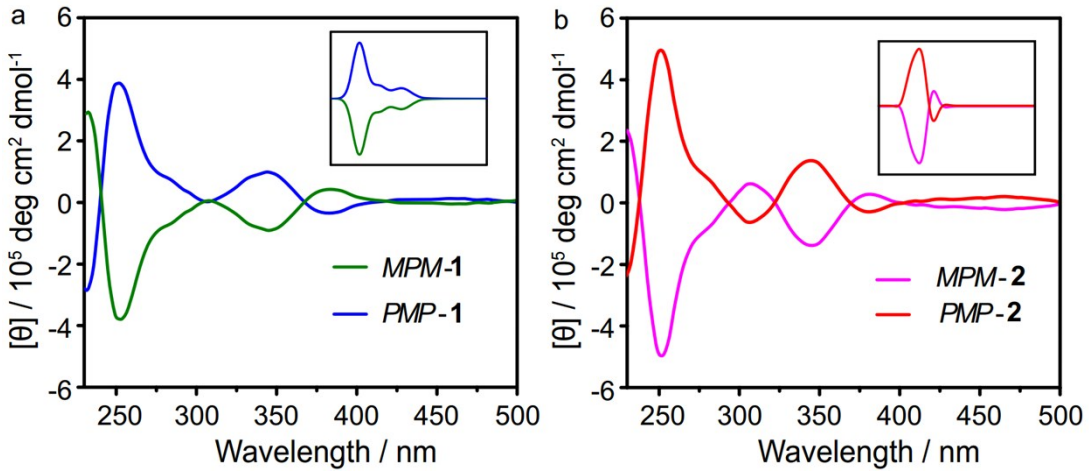

Figure S11. Experimental and (ZINDO/S)-predicted (the insert) CD spectra of *MPM*-**1** (green) and *PMP*-**1** (blue) (a), *MPM*-**2** (red) and *PMP*-**2** (purple) (b).

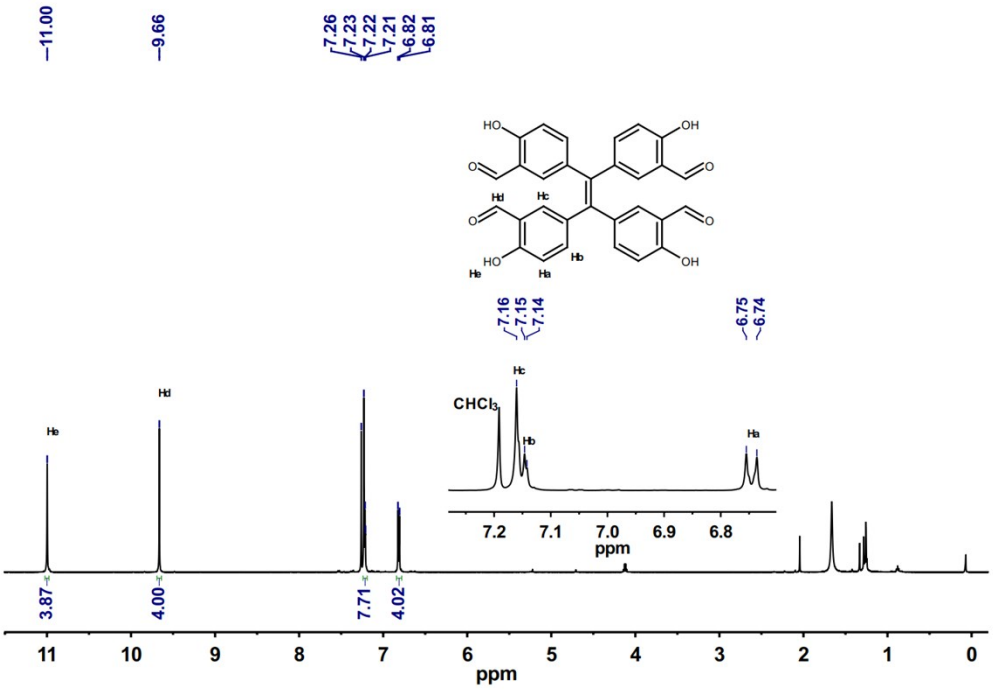

Figure S12. ^{1}H-NMR of THFPE (500 MHz) exhibited only one peak for aldehyde group, revealing the high freedom of phenyl rings in solution.

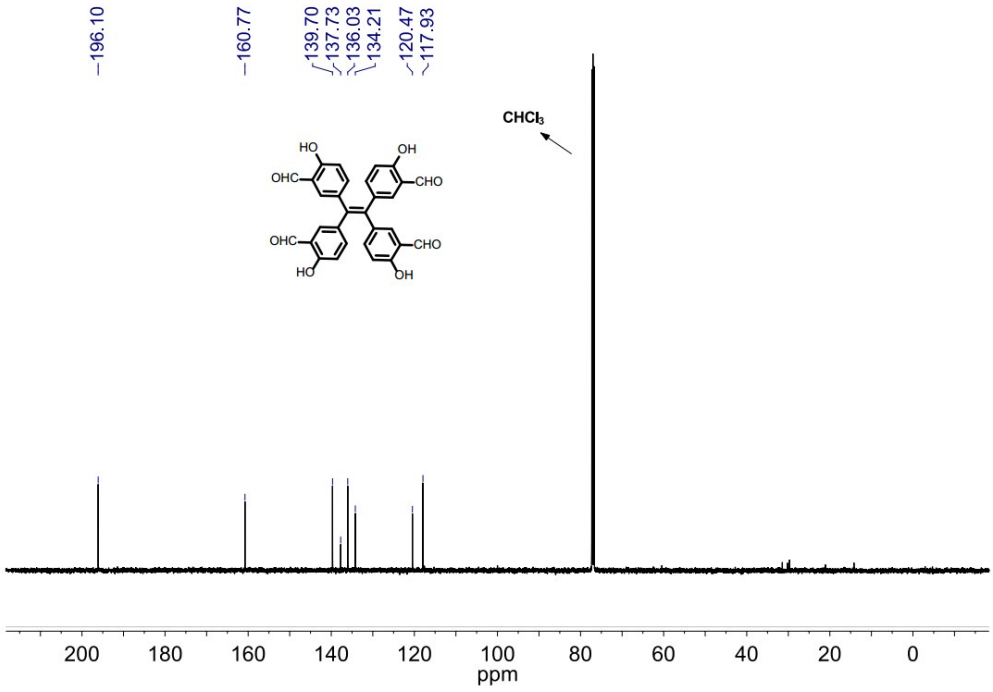

Figure S13. ^{13}C-NMR of THFPE (125 MHz) in $CDCl_3$.

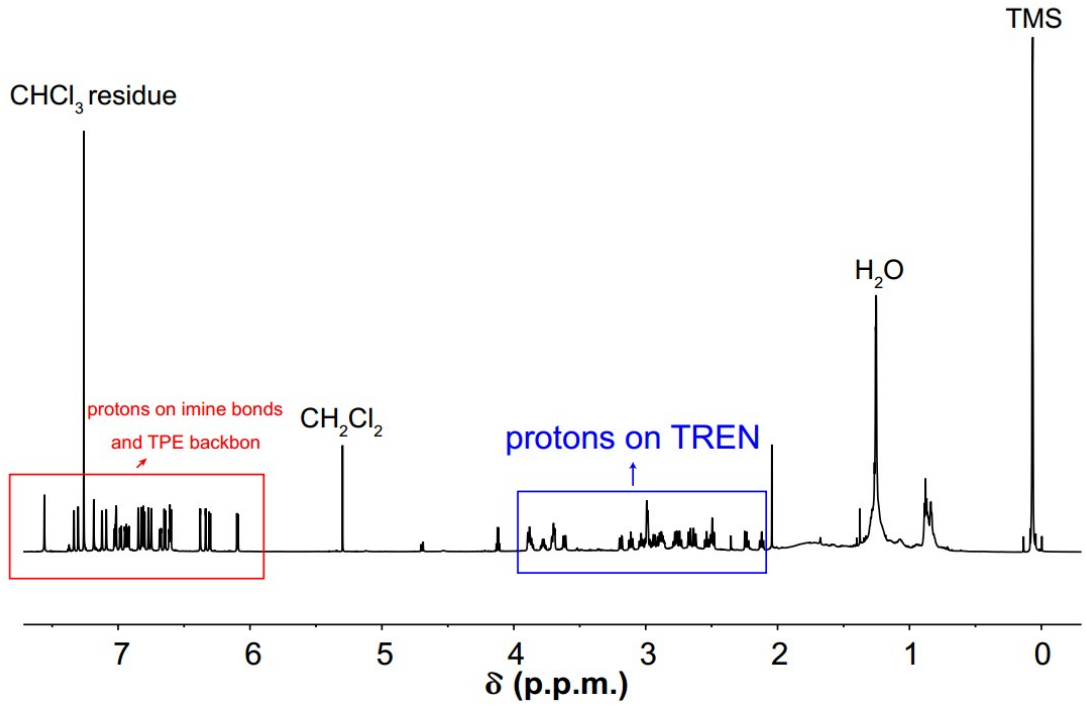

Figure S14. The whole [1]H-NMR (850 MHz) spectrum of *PMP*-**1**. Detailed assignment of each proton is in the Figure S16-S17.

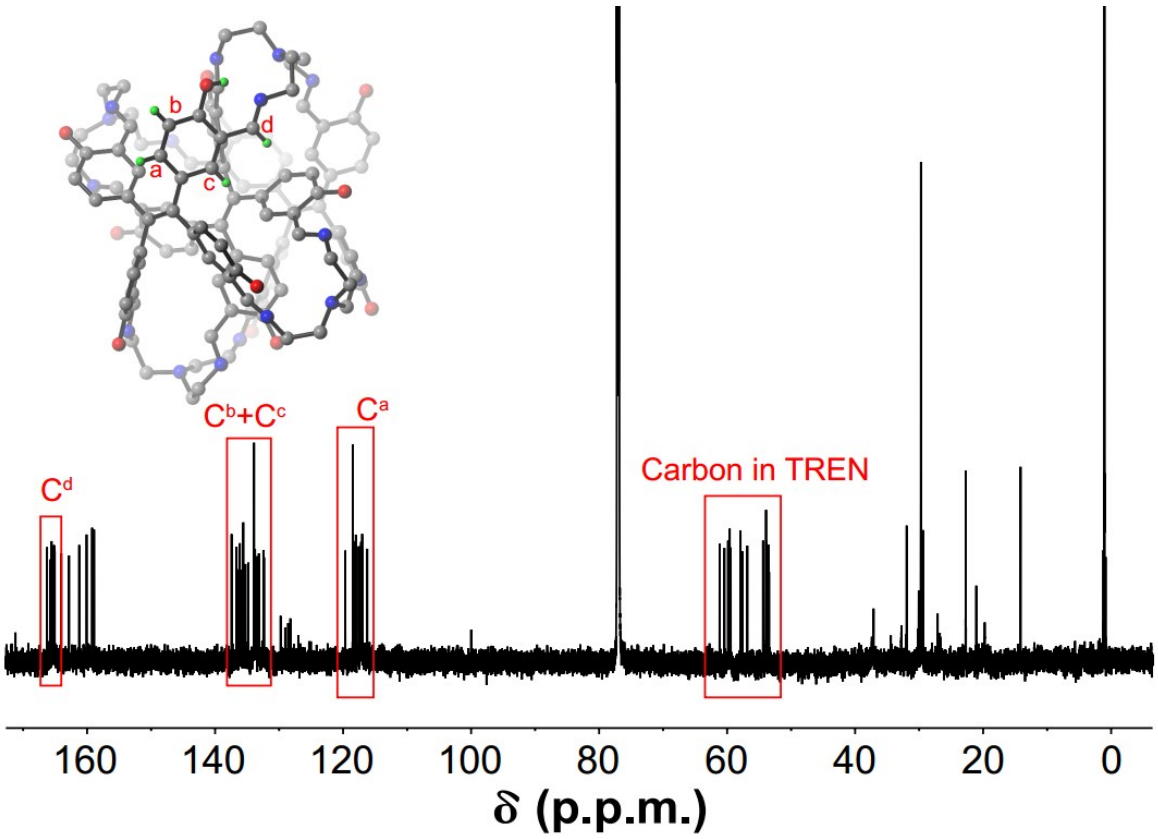

Figure S15. The whole [13]C-NMR (213 MHz) spectrum of *PMP*-**1**. Detailed assignment of each proton is in the Figure S16-S17.

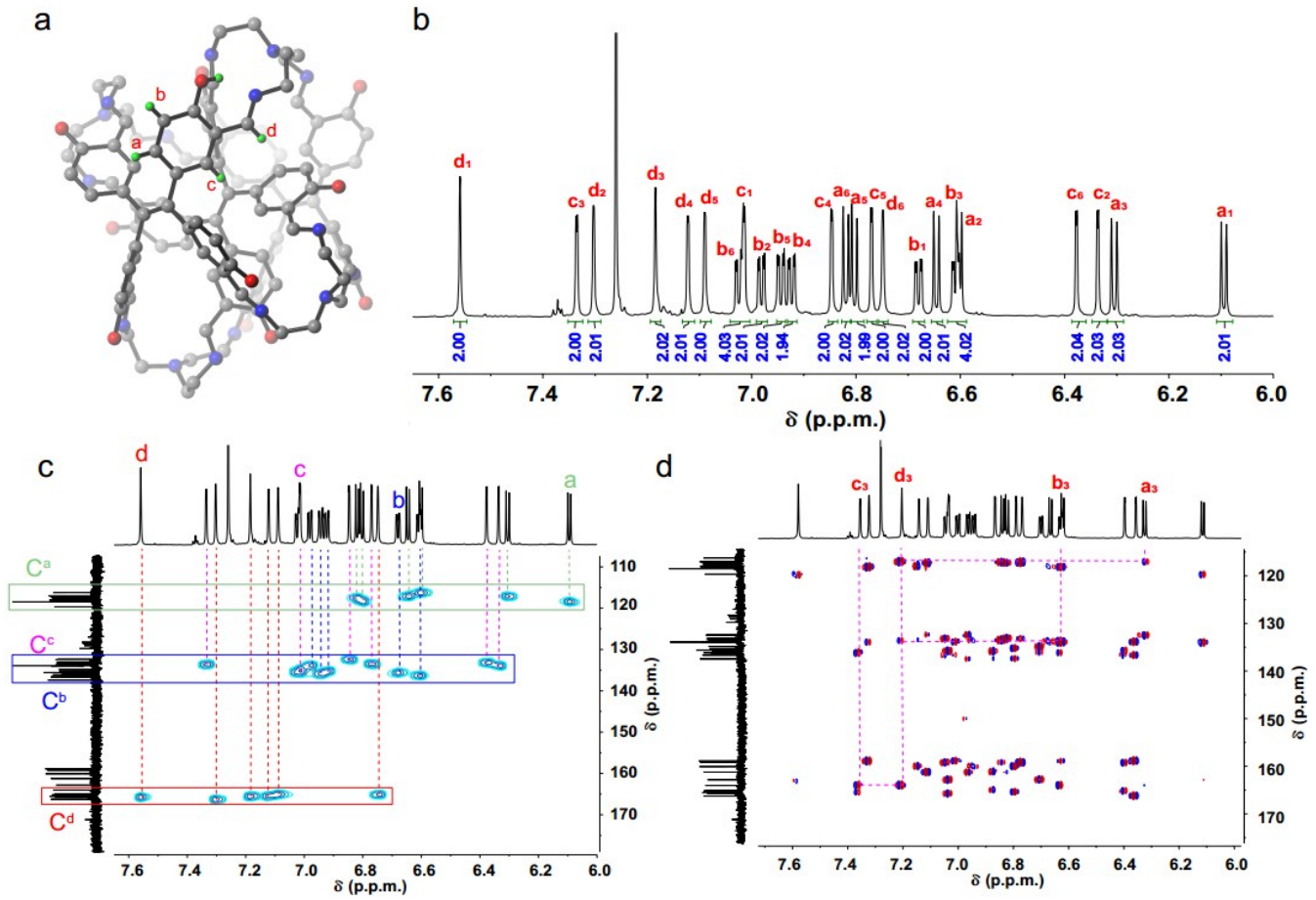

Figure S16. The assignment of ^{1}H-NMR (850 MHz) for each proton in TPE backbone of *PMP*-**1**. There are four typical protons in TPE backbone, namely H^a, H^b, H^c, H^d as presented in the molecular structure (a). Only six sets of protons exist in ^{1}H-NMR spectrum, indicating the C_2-symmetry **FRSs** in solution (b). Four protons were closely related to four unique regions of carbon resonance signals in HSQC spectrum, which helped us to determine the types of protons (c). HMBC spectrum allows for the assignment of protons in one phenyl set (d, only one representative Set 3 was shown for clarity).

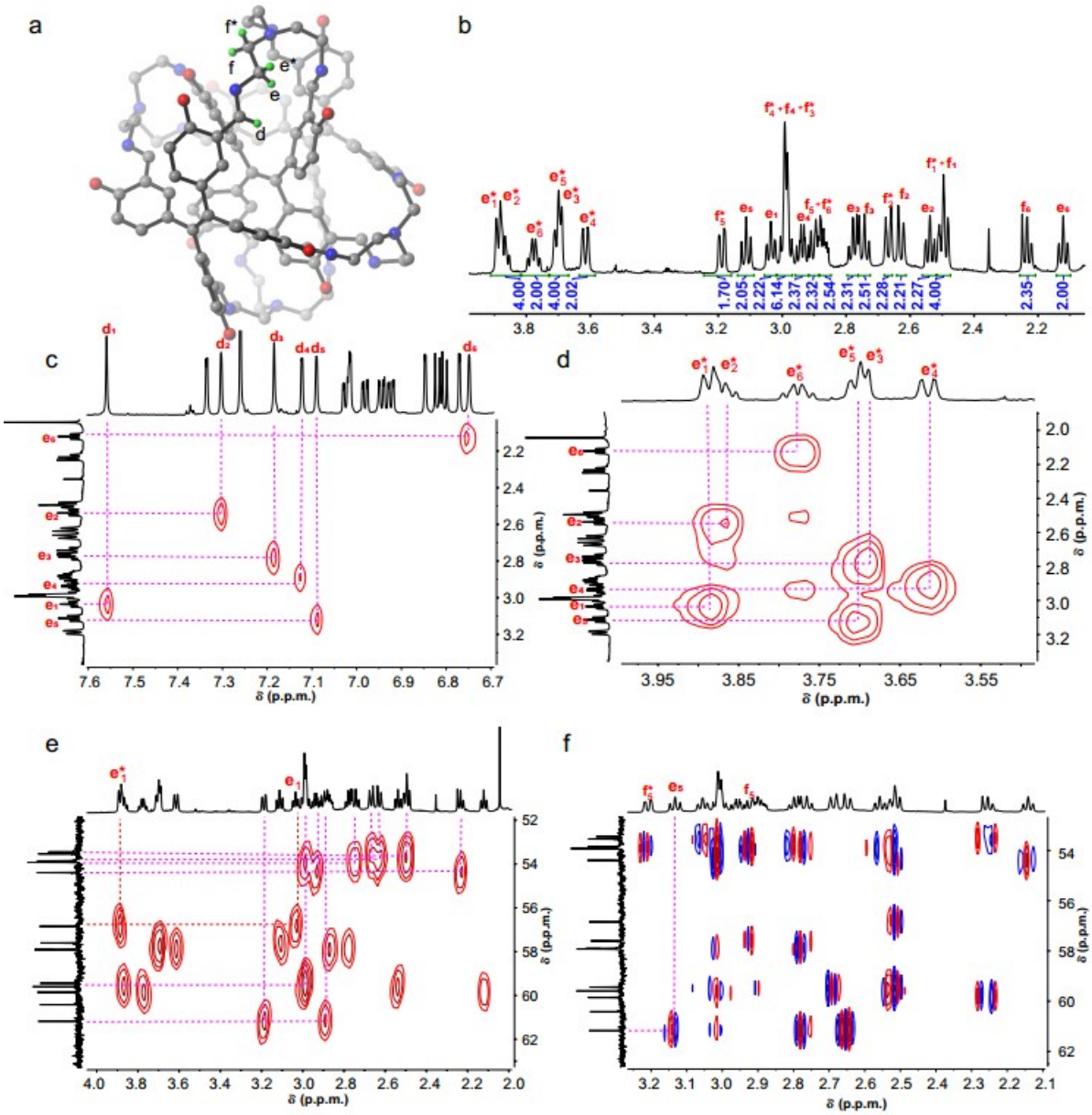

Figure S17. The assignment of ^{1}H-NMR (850 MHz) for each proton in TREN vertices of *PMP*-**1**. There are five typical protons in vertices, namely H^{d}, H^{e}, H^{e*}, H^{f}, H^{f*}, as presented in the molecular structure (a). Only six sets of protons exist in ^{1}H-NMR spectrum, indicating the C_2-symmetry **FRSs** in solution (b). The NOE crosspeaks between H^{e} and H^{d} reflected the *E* conformation of imine bonds and the structural rigidity of *PMP*-**1** (c). Two protons of methylene in TREN (H^{e} and H^{e*}), are in distinct chemical environment and split into two individual peaks, confirming the non-covalent repulsive interactions restrict the movement of flexible TREN in solution (d). HSQC (e) and HMBC (f) spectra helped us to determine the protons in one alkyl chain. (Only two representative Set 1 and Set 5 were shown for clarity)

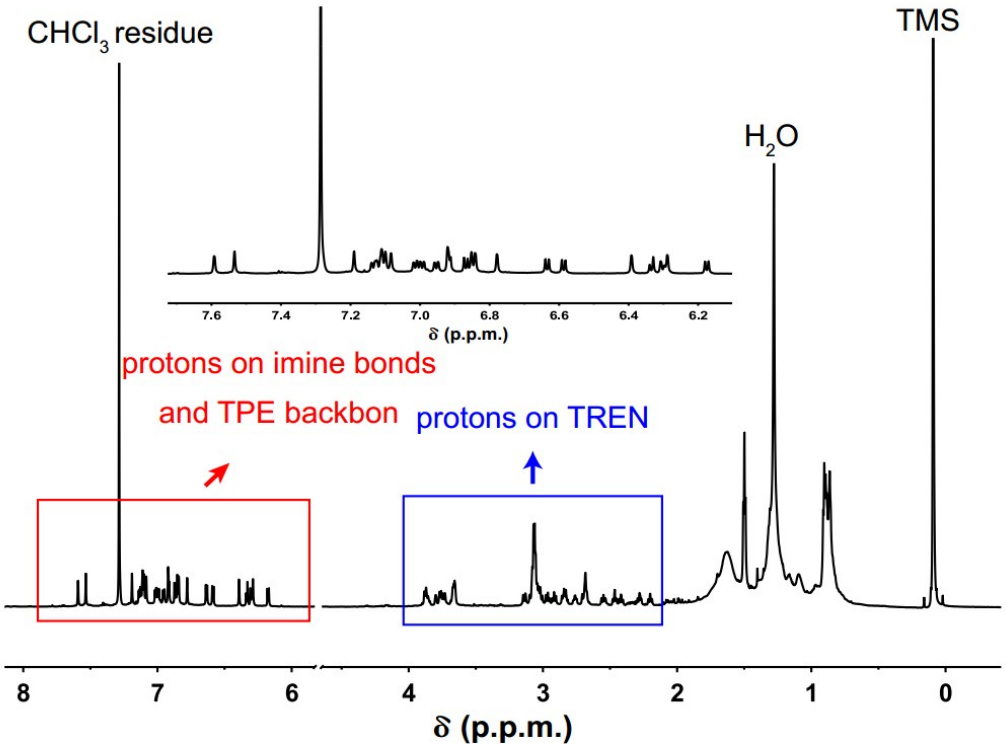

Figure S18. The whole ^{1}H-NMR (850 MHz) spectrum of *PMP*-**2** and the details of proton signals in aromatic region (the insert). However, due to small ratio of *PMP*-**2** in the mixture, we failed to achieve enough samples to obtain high-quality ^{13}C-NMR spectrum and other 2D NMR spectra.

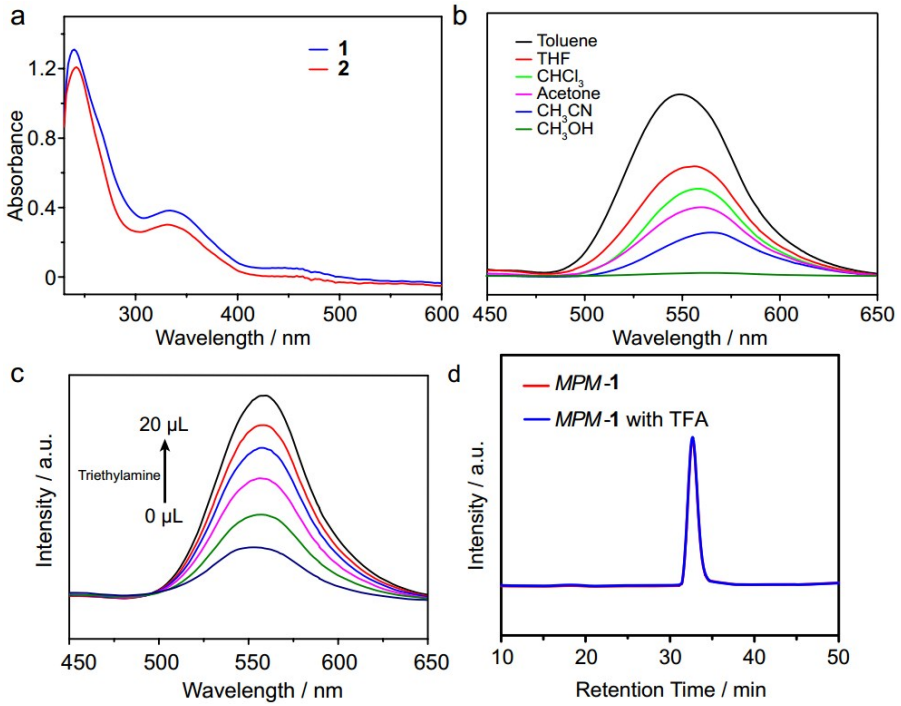

Figure S19. a. UV-vis spectra of **FRSs 1** (10 μM, blue) and **2** (10 μM, red) in dichloromethane. b. the fluorescence spectra of **1** (10 μM) in various solvent. (excited at 360 nm). c. the fluorescence can recover to the initial intensity by using trimethylamine to neutralize TFA. d. HPLC spectrum of *MPM*-**1** in present of TFA is same as that of *MPM*-**1**, indicating imine bonds in **FRSs** is stable against acid.

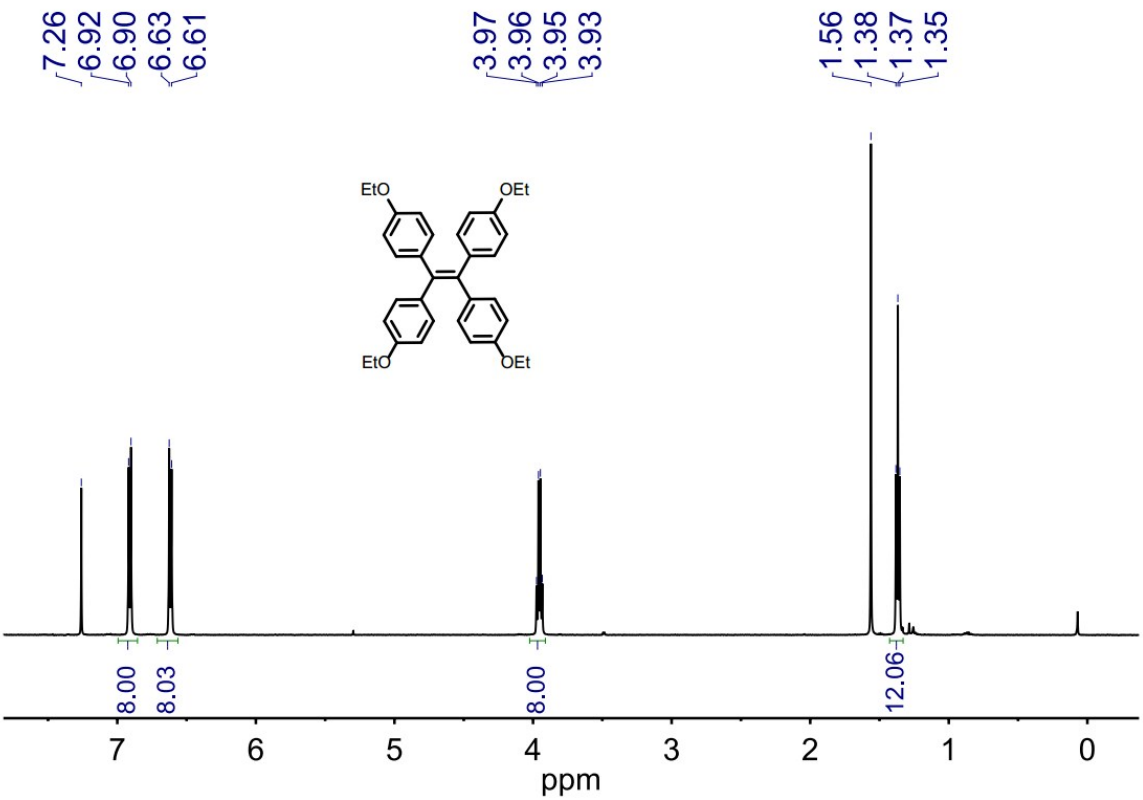

Figure S20. The ^{1}H-NMR (500 MHz) spectrum of compound 3.

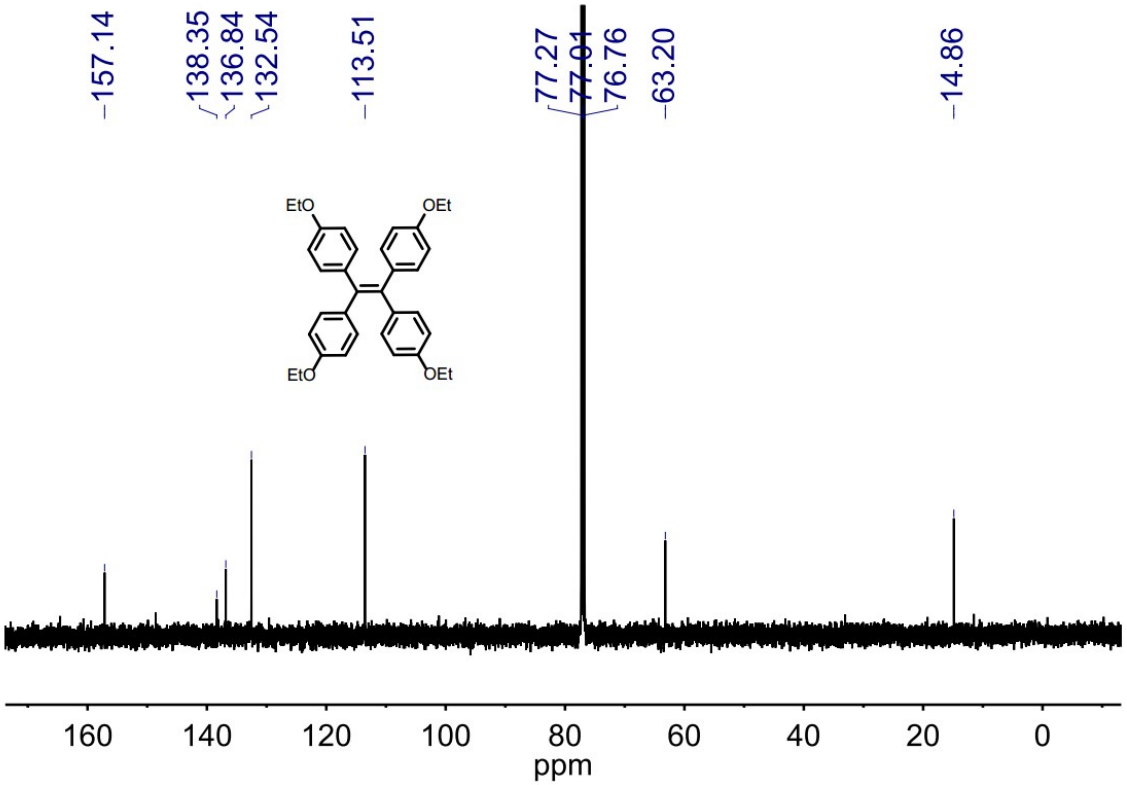

Figure S21. The ^{13}C-NMR (125 MHz) spectrum of compound 3.

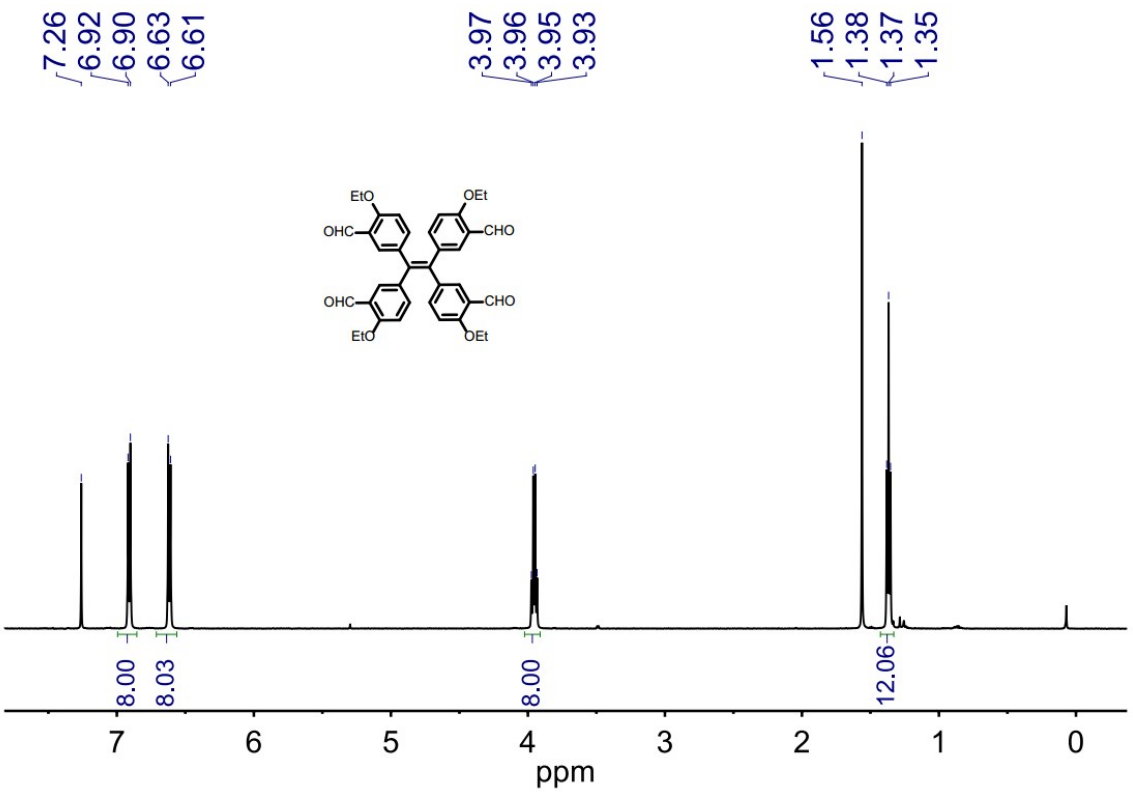

Figure S22. The ^{1}H-NMR (500 MHz) spectrum of TOEPE.

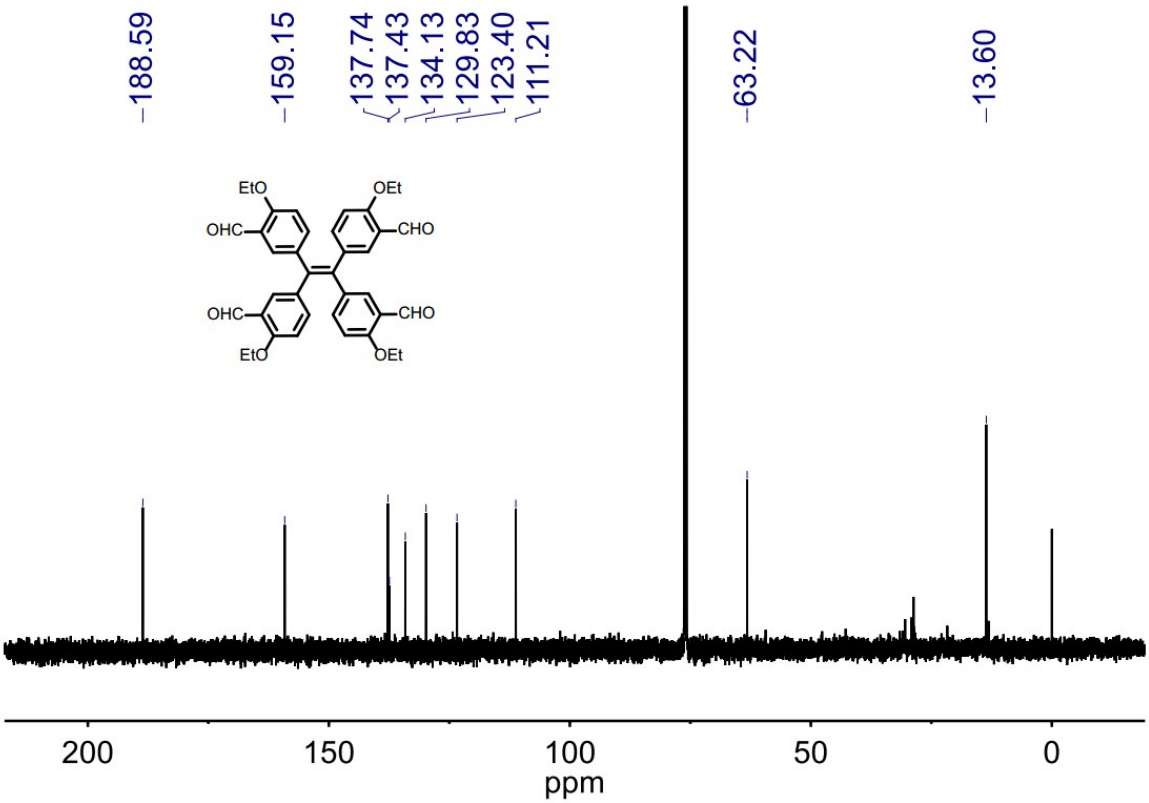

Figure S23. The ^{13}C-NMR (125 MHz) spectrum of TOEPE.

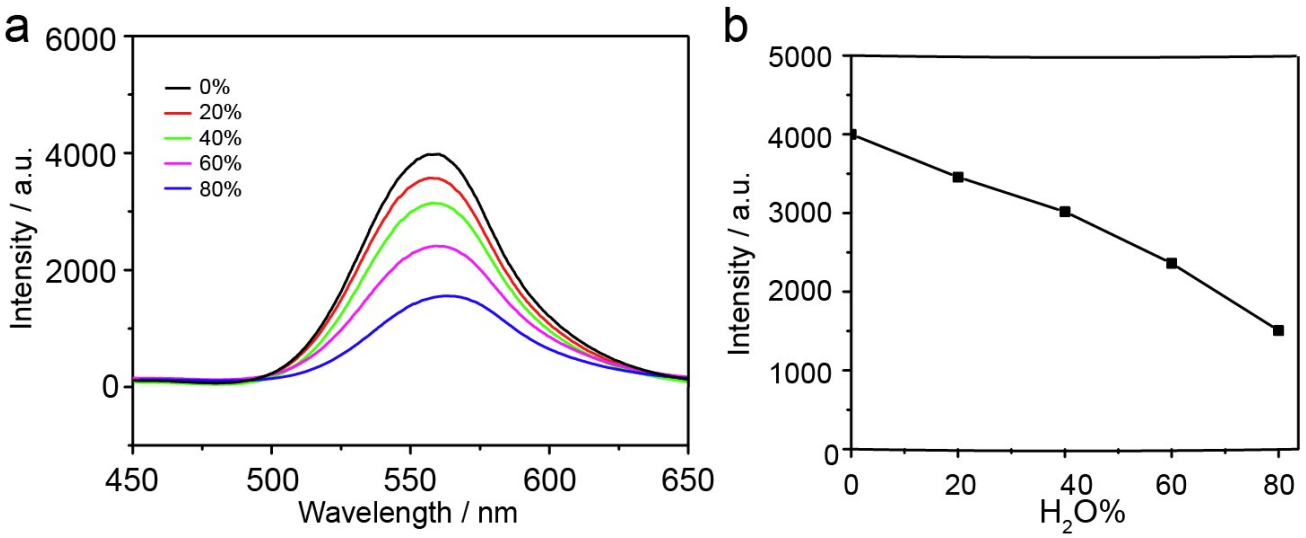

Figure S24. Increasing the ratio of water (poor solvent) in THF from 0% to 80% resulted in decrease of the fluorescent intensity of **FRSs 1**. The decrease of fluorescence intensity can be rationalized by the increase of polarity of mixed solvent.

Table S1 Crystal data and structure refinement for **FRSs**

FRSs	**1**	**2**
Empirical formula	$C_{114}H_{108}N_{16}O_{12}$	$C_{114}H_{108}N_{16}O_{12}$
Formula weight	1894.16	1894.16
Temperature (K)	150.00(10)	150.00(10)
Crystal system	Monoclinic	Orthorhombic
Space group	*P*2/*c*	*Pccn*
a(Å)	26.0567(5)	19.0205(3)
b(Å)	14.2086(3)	20.3813(4)
c(Å)	28.6868(6)	30.1755(5)
α (deg)	90	90
β (deg)	94.091(2)	90
γ (deg)	90	90
V(Å^3)	10593.6(4)	11697.9(4)
Z	4	4
ρ_{cal} (g·m^{-3})	1.188	1.076
μ(mm^{-1})	0.632	0.572
F(000)	4000	4000
Crystal size (mm)	0.2×0.2×0.2	0.2×0.2×0.2
Radiation	CuK_α (λ =1.54184 Å)	CuK_α (λ =1.54184 Å)
2Θ range for data collection (deg)	7.09 to 141.8	5.858 to 147.382
Index ranges	-22 ≤ h ≤ 31, -17 ≤ k ≤ 12, -29 ≤ l ≤ 34	-23 ≤ h ≤ 17, -25 ≤ k ≤ 18, -36 ≤ l ≤ 36
Reflections collected	34160	41067
Independent reflections	19489 [R_{int} = 0.0356, R_{sigma} =0.0478]	11538 [R_{int} = 0.0278,R_{sigma} =0.0267]
Data/restraints/parameters	19489/0/1291	11538/0/646
Goodness-of-fit on F^2	1.013	1.072
Final *R* indexes [$I>2\sigma(I)$]	R_1= 0.0576, wR_2 = 0.1504	R_1= 0.0540, wR_2 = 0.1610
Final *R* indexes (all data)	R_1 = 0.0810, wR_2 = 0.1668	R_1 = 0.0634, wR_2 = 0.1688
Largest diff. peak/hole(e Å^{-3})	0.42/-0.33	0.49/-0.21

Synthesis of compound 3: Zn (10.4 g, 160mmol) powder was suspended in THF (250 mL) and $TiCl_4$ (16 mL, 15.2 g, 80 mmol) was added dropwise at 0 ℃ in several minutes. The reaction was kept at 0 ℃ for 30 min and the mixture was refluxed for another 2 h. Then pyridine (4 mL) was added at 0 ℃ and the mixture was stirred for 30 min. Compound 2 (10.8 g, 40 mmol) was dissolved in THF (60 mL) and added into the solution. The mixture was heated to reflux for 20 h. The solution of $NaHCO_3$ in water was added to quench the reaction, and the crude product was extracted by DCM and purified by silica gel with PE/EA (10/1 vol.) eluent to afford compound 3 (7.6 g) as yellow solid in 75% yield. ^{1}H-NMR (500 MHz, $CDCl_3$): δ 6.91 (d, J = 8.7 Hz, 8H), 6.62 (d, J = 8.7 Hz, 8H), 3.95 (q, J = 7.0 Hz, 8H), 1.37 (t, J = 7.0 Hz, 12H).^{13}C -NMR (125 MHz, $CDCl_3$): δ 157.14, 138.35, 136.84, 132.54, 113.51, 77.27, 77.01, 76.76, 63.20, 14.86. HRMS (m/z): $[M+Na]^+$ calcd for $[C_{34}H_{36}O_4Na]^+$ 531.2511, found 531.2505.

Synthesis of TOEPE: Hexamethylenetetramine (1.1 g, 8 mmol) were added into the solution of compound 3 (1.0 g, 2.0 mmol) in trifluoroacetic acid (35 mL). The solution was refluxed for 8 h and then cold water and DCM were added into the solution. The mixture was stirred for another 4 h at room temperature and extracted with DCM. The combined organic phase was dried over anhydrous sodium sulfate, filtered and evaporated to dryness. The crude product was purified by silica gel with PE/EA (3/1 vol.) eluent to afford TOEPE (0.89 g) as yellow solid in 72% yield. ^{1}H-NMR (500 MHz, $CDCl_3$): δ 10.34 (s, 4H), 7.43 (d, J = 2.3 Hz, 4H), 7.15 (dd, J = 8.6, 2.3 Hz, 4H), 6.70 (d, J = 8.7 Hz, 4H), 4.08 (d, J = 7.0 Hz, 8H), 1.43 (t, J = 7.0 Hz, 12H).^{13}C NMR (125 MHz, $CDCl_3$): δ 188.59, 159.15, 137.74, 137.43, 134.13, 129.83, 123.40, 111.21, 63.22, 13.60. HRMS (m/z): $[M+Na]^+$ calcd for $[C_{38}H_{36}O_8Na]^+$ 643.2307, found 643.2310 .

Synthesis of THFPE: TOMPE (1.2 g, 2 mmol) was dissolved by using DCM (30 mL) in a dried two-neck flask and BBr_3 (1.85 mL, 5 g, 20 mmol) diluted by DCM (50 mL) was added into the solution dropwise at 0 ℃. After reaction stirred at room temperature for 15 h, water was added to the flask and the crude product was extracted by EA and organic phase was dried over anhydrous sodium sulfate, filtered and evaporated to dryness. The crude product was purified by silica gel with PE/EA (3/1 vol.) eluent to afford THFPE (0.99 g) as yellow solid in 98% yield. ^{1}H NMR (500 MHz, $CDCl_3$): δ 11.00 (s, 4H), 9.66 (s, 4H), 7.24-7.19 (m, 8H), 6.81 (d, J = 9.3 Hz, 4H). ^{13}C NMR (125 MHz, $CDCl_3$): δ 196.10, 160.77, 139.70, 137.73, 136.03, 134.21, 120.47, 117.93. HRMS (m/z): $[M+Na]^+$ calcd for $[C_{30}H_{20}O_8Na]^+$ 531.1055, found 531.0944 .[1]

Synthesis of FRSs: THFPE (61 mg, 0.12 mmol), TREN (tris(2-aminoethyl)amine, 23.4 mg, 0.16 mmol) and dry TFA(trifluoroacetic acid, 0.45 mg, 4μmol) were reacted in $CHCl_3$ (30 mL) at 45 ℃ for 5 d to afford yellow solution for further HPLC separation. And the yield of **FRSs** was calculated to be 97.6 % according to HPLC data (Figure S5).

The details for HPLC and CD experiment of FRSs: The HPLC separation was employed the Daicel Chiralpak IE Column on a Shimadzu LC-16A instrument at a flow rate of 0.5 mL min^{-1}, by using the mobile phase of chloroform-toluene-methanol (1:1:2, vol., before 25 min) and chloroform-methanol (3:2, vol., after 25 min) with 0.2% diethylamine.

CD and UV-vis analyses of each separated stereoisomers were measured in dichloromethane at the concentration of 10 μM.

Single-crystal X-ray diffraction. Slow evaporation of each separated fraction in chloroform was allowed to afford the prismatic crystals after a month. However, only racemic crystals were obtained because of the racemization of each diastereoisomer.

Single crystal X-ray diffraction data were collected on Rigaku SuperNova X-Ray single crystal diffractometer using Cu K_α (λ = 1.54184 Å) micro-focus X-ray sources. The suitable crystals were collected, covered with protective oil and mounted on X-ray diffractometer at 150 K.

The raw data were collected and reduced by CrysAlisPro software. The structures were solved by the SHELXT[2] with Intrinsic Phasing and refined on F^2 by full-matrix least-squares methods with the SHELXL[2] and OLEX2[3] was used as GUI. The detailed crystal parameters are listed in the Supplementary Tab. 1.

Refinement details: For each crystal of **FRSs 1** and **2**, all nonhydrogen atoms were refined anisotropically. Hydrogen atoms were placed at calculated positions using the riding model and refined isotropically. The instructions AFIX 23 and AFIX 43 were used for the hydrogen atoms on the secondary -CH_2- and the aromatic C-H, respectively, with the parameter of U_{iso} = 1.2 U_{eq}. A satisfactory disorder model for the solvent molecules was not found, therefore the OLEX2 Solvent Mask routine (similar to PLATON/SQUEEZE) was used to mask out the disordered density.

3. Computational Section

Calculation of CD spectra: CD spectra were calculated at ZINDO[4,5] semi-empirical level with Gaussian 09[6] and used the optimized crystal structures of **FRSs**. The electronic transitions were then fitted to a Lorentzian distribution to generate the spectra.

DFT calculation: The restriction of phenyl flipping lead to inherent *P* or *M* helical chirality of the TPE faces in **FRSs**. However, it remains an open question why **FRSs** take the alternating packing mode of *P* or *M* configurations. In **FRSs**, we found two types of non-covalent repulsive interactions in TREN vertices could influence the rotational patterns of TPE faces. The first type is repulsive interactions among the three alkyl chains of TREN, and the second one is repulsive interactions of atoms in the same alkyl chain. Therefore, we constructed a C_2-symmetric structure of *PPP*-**1** through substituting the middle *M* face into *P* face in *PMP*-**1**. The DFT calculation was performed to optimize the structure of *PPP*-**1**. The energy of structure of *PPP*-**1** is 1648.30 kJ mol^{-1} higher than that of *PMP*-**1**. Moreover, in the optimized structure of *PPP*-**1**, TREN has the extremely distorted conformation rather than the anti-clockwise rotational configuration in *PMP*-**1**. This suggested the first repulsive interactions lead to anti-clockwise rotational configurations of TREN. In addition, the torsion angle (θ, Figure S8) in N-C-C-N gauche conformation of *PMP*-**1** is 63°. Whereas θ in *PPP*-**1** is 13°, which can significantly increase the second type of repulsive forces. Therefore, we varied θ from 0° to 180° in one alkyl chain to construct the potential energy surfaces (PES). In PES, the structures have the lowest energy in 65°, which is consistent with the crystal structure of *PMP*-**1**. The second type of repulsive interactions restricted the movement of alkyl chains and thus transfer the chirality from rotational conformations of TREN to TPE entities, resulting in facial hetero-directionality in **FRSs**.

The details of DFT calculation: All the structural optimization and energy calculation were carried out by DFT using the M06 functional[7] with the effective core potential and basis set TZP, an ultrafine integration grid and tight geometrical convergence criteria (Geometry Convergence energy change 10^{-3} Hatree; constrained gradient max: 10^{-3} Hatree/Å; constrained gradient rms: 6.6667×10^{-3} Hatree/Å; cart. step max: 10^{-2} Å; cart. step rms: 6.6667×10^{-3} Å) with the Gaussian 09 package. The solvation terms were calculated by the COSMO solvation model[8], which assumes a dielectric medium around a gas-phase structure of molecule, and minimizes the energy of the molecule within this medium.

4. Reference

1. J. B. Xiong, H. T. Feng, J. P. Sun, W. Z. Xie, D. Yang, M. Liu and Y. S. Zheng, *J. Am. Chem. Soc.*, **2016**, *138*, 11469-11472.
2. Sheldrick, G. M. *Acta Crystallogr. Sect. C*, **2015**, *71*, 3-8.
3. Dolomanov, O. V.; Bourhis, L. J.; Gildea, R. J. K.; Puschmann, H. J. *Appl. Crystallogr*. **2009**, *42*, 339-341.
4. Telfer, S. G.; Tajima, N.; Kuroda, R.; Cantuel, M.; Piguet, C. *Inorg. Chem.* **2004**, *43*, 5302-5310.
5. Telfer, S. G.; Tajima, N.; Kuroda, R. *J. Am. Chem. Soc.,* **2004**, *126*, 1408-1418.
6. Frisch, M.; Trucks, G.; Schlegel, H.; Scuseria, G.; Robb, M.; Cheeseman, J.; Scalmani, G.; Barone, V.; Mennucci, B.; Petersson, G.; Nakatsuji, H.; Li, X.; Caricato, M.; Marenich, A. V.; Bloino, J.; Janesko, B. G.; Gomperts, R.; Mennucci, B.; Hratchian, H. P.; Ortiz, J. V.; Izmaylov, A. F.; Sonnenberg, J. L. Gaussian 09 revision B.01. **2010**.
7. Y. Zhao; D.G. Truhlar, *Theor. Chem. Acc.,* **2008**, *120*, 215-241
8. A. Klamt; G. Schüürmann, *J. Chem. Soc., Perkin Trans.,* **1993***, 2*, 799